

# Calibration and Validation of the RapidScat Scatterometer Using Tropical Rainforests

Nathan M. Madsen, *Member, IEEE*, and David G. Long, *Fellow, IEEE*

**Abstract**—Launched in September 2014, RapidScat is currently operating on the International Space Station (ISS). RapidScat estimates ocean vector winds via the measurement of the normalized radar coefficient ( $\sigma^0$ ) of the ocean's surface. Measurements are also collected over land. The ISS orbit permits, for the first time, the observation of the diurnal variation in Ku-band  $\sigma^0$  at mid- to high-incidence angles. To complement calibration efforts over the ocean, in this paper the calibration and validation of the  $\sigma^0$  measurements are performed using natural land targets, namely the Amazon and Congo rainforests. The diurnal  $\sigma^0$  cycle of the targets is estimated with respect to incidence angle, azimuth angle, and season using measurements from previous sensors. Understanding this diurnal backscatter response enables the comparison of RapidScat measurements with measurements from the QuikSCAT, NASA Scatterometer, SeaWinds, and Oceansat-II scatterometers. RapidScat  $\sigma^0$  measurements are found to be consistent but biased low compared to those of QuikSCAT by up to 0.3 dB. The effectiveness of slice balancing is evaluated and found to be dependent on the pitch of the ISS. Extreme pitches of the ISS are also found to introduce azimuth dependencies in egg measurements. By accounting for seasonal and diurnal cycles, we find that the rainforests are well suited for scatterometer sensor cross-calibration, even for disjoint years.

**Index Terms**—Calibration, QuikSCAT, RapidScat, scatterometer.

## I. INTRODUCTION

WIND scatterometers are spaceborne radar systems designed to accurately measure the normalized radar cross section ( $\sigma^0$ ) of the Earth. The primary application for these  $\sigma^0$  measurements is vector wind retrieval over the ocean [1], but there also are applications over both land and ice.

The latest Ku-band scatterometer, RapidScat, was launched in September 2014 aboard a Falcon 9 rocket and mounted on the International Space Station (ISS), from which it is currently operating. RapidScat uses spare hardware created during the development of the SeaWinds scatterometer and thus is nearly identical to the previous SeaWinds scatterometers launched on the QuikSCAT (prime wind mission 1999–2009) and Advanced Earth Observing System (ADEOS-II (2002) platforms [2]–[4]. The processing software is also nearly identical. The major difference between RapidScat and the previous SeaWinds scatterometers is the platform and orbit. The nature of the ISS as a platform presents new challenges for accurate  $\sigma^0$  measurement.

Manuscript received September 26, 2015; revised November 7, 2015; accepted December 1, 2015. Date of publication December 29, 2015; date of current version March 25, 2016.

The authors are with the Department of Electrical and Computer Engineering, Brigham Young University, Provo, UT 84602 USA (e-mail: long@ee.byu.edu).

Color versions of one or more of the figures in this paper are available online at <http://ieeexplore.ieee.org>.

Digital Object Identifier 10.1109/TGRS.2015.2506463

Postlaunch calibration and validation activities ensure that the scatterometer is working properly and that its measurements are accurate and consistent with previous scatterometers. Considerable work has been done in calibrating and validating the retrieved vector winds over the ocean using *in situ* measurements, other sensors, and climate models. In this paper, we focus on the direct calibration of  $\sigma^0$  using distributed land regions as calibration targets to validate the RapidScat  $\sigma^0$  measurements and cross-calibrate them with prior Ku-band scatterometers in order to continue the Ku-band land  $\sigma^0$  climate record.

The calibration and validation for scatterometers using natural land targets such as the Amazon rainforest have been performed for much of the history of scatterometry. The Amazon rainforest was first proposed as a calibration target in [5] after considering measurements from the Seasat scatterometer and Skylab. It was found that the Amazon is temporally quite stable and has minimal azimuth dependence. The Amazon rainforest response was used to propose time-, beam-, and cell-dependent corrections for Seasat data [6]. The Amazon rainforest has also been used in beam balancing for the NASA Scatterometer (NSCAT) [7], [8], beam and slice balancing in QuikSCAT [4], [9], intercalibration between QuikSCAT and SeaWinds on ADEOS-II [10], and intercalibration between QuikSCAT and the Oceansat-II Scatterometer (OSCAT) [11]–[13]. In most of these studies, an additional region is used to confirm the results from the Amazon. We follow this precedent by using the Amazon and Congo rainforests. We focus on quantifying instrumental biases with respect to QuikSCAT. QuikSCAT is chosen because of its decade-long consistent data set.

Even in the relatively homogeneous and temporally stable rainforests, there are still natural variations in the  $\sigma^0$  response that must be accounted for when calibrating the scatterometer [14], [15]. In this paper, measured  $\sigma^0$  from various Ku-band scatterometers are used to develop simple empirical models for the responses of our targets to factors such as incidence angle, azimuth angle, time of year (season), and local time of day (ltod). These models are used during the calibration and validation of RapidScat to compensate for differences in target response when comparing measurements. Notably, the orbit of RapidScat enables, for the first time, the spaceborne observation of the full diurnal variation in Ku-band  $\sigma^0$  at mid- to high-incidence angles for natural land targets. This provides a unique opportunity for studying the geophysical processes contributing to the observed diurnal cycles in  $\sigma^0$  and aids in the cross-calibration between sensors that have collected measurements at distinct ltod.

We evaluate the consistency of RapidScat  $\sigma^0$  measurements over its mission life. Particular areas of concern are long-term

TABLE I  
SUMMARY OF KEY FEATURES OF EACH SCATTEROMETER AND ITS DATA SET. LOCAL TIME IS THE LTOD AT THE EQUATOR CROSSINGS. "ASC" REFERS TO THE ASCENDING NODE (NORTH-BOUND EQUATOR CROSSING), WHILE "DESC" REFERS TO THE SOUTH-BOUND EQUATOR CROSSING

Parameter	NSCAT	QuikSCAT	QSCAT PWM	SeaWinds	OSCAT	RapidScat
Duration	Aug 1996 - Jun 1997	Jun 1999 - Nov 2009	Nov 2009 - Present	Dec 2002 - Oct 2003	Oct 2009 - Mar 2014	Sep 2014 - Present
Frequency	14.0 GHz	13.4 GHz	13.4 GHz	13.4 GHz	13.5 GHz	13.4 GHz
Incidence Ang.	10°-55° HH 10°-55° VV	46.25° HH 54° VV	Various	46.25° HH 54° VV	49° HH 57° VV	47-50.5° HH 53-57° VV
Azimuth Ang.	Fixed	All	Various	All	All	All
Local Time	10 p.m. Asc 10 a.m. Desc	6 a.m. Asc 6 p.m. Desc	6 a.m. Asc 6 p.m. Desc	10 p.m. Asc 10 a.m. Desc	12 a.m. Asc 12 p.m. Desc	All

$\sigma^0$  drift and so-called "slice balancing" [9]. RapidScat collects both low-resolution  $\sigma^0$  measurements, termed "eggs," and higher resolution measurements, termed "slices." The former are defined by the antenna footprint on the surface, while the latter are created via range-Doppler processing [16]. Small azimuthally dependent biases in slice  $\sigma^0$  measurements were found and corrected when validating QuikSCAT [4], [9] and thus are investigated in this paper. We also evaluate the consistency of  $\sigma^0$  measurements with respect to attitude changes, an issue of particular importance with the ISS, which has a higher attitude variability than previous platforms used for SeaWinds instruments.

## II. DATA SETS USED

Five Ku-band scatterometer data sets are considered in this paper. All but RapidScat have been previously calibrated. The primary features of interest for each of the data sets mentioned are summarized in Table I.

The earliest data set is from NSCAT. NSCAT was launched in August 1996 aboard the Japanese Advanced Earth Observing Satellite [1] and operated until June 1997 to yield a 10-month data set. NSCAT operated at 13.995 GHz in the Ku-band and had a fan-beam configuration for its antennas. The fan-beam design yielded measurements at a wide range of incidence angles and is well calibrated [7], [8], making NSCAT a good choice for measuring incidence dependence.

The SeaWinds scatterometer on QuikSCAT (henceforth referred to as QuikSCAT) was launched in June 1999 and measured winds until November 2009 when the antenna stopped scanning due to a worn bearing. QuikSCAT's data set is the longest continuous Ku-band data set available. QuikSCAT operated at 13.4 GHz and had two rotating pencil-beam antennas at fixed incidence angles [3].

After November 2009, QuikSCAT entered what is termed the postwind mission (PWM) mode. Although unable to scan in azimuth, it continues to measure  $\sigma^0$  with a narrow swath. To refine the geophysical model function that relates  $\sigma^0$  to vector winds, the QuikSCAT spacecraft attitude was adjusted to different attitudes for months at a time to collect  $\sigma^0$  measurements at different incidence and azimuth angles [17]. The PWM data used in this paper are provided by the Jet Propulsion Laboratory (JPL) as "Repointed QuikSCAT files."

The second SeaWinds scatterometer (henceforth referred to as SeaWinds) operated on ADEOS-II from December 2002 to September 2003 [2]. SeaWinds is nearly identical to QuikSCAT except for the ltod of its measurements.

Built by the Indian Space Research Organization and operated from October 2009 to March 2014, OSCAT shared a similar pencil-beam design with QuikSCAT and SeaWinds but had different nominal incidence angles and acquired measurements at a different ltod.

RapidScat was launched in September 2014 and is currently operational. The instrument hardware is almost identical to that of QuikSCAT and SeaWinds since it was originally built as an engineering model during the development of those two instruments. RapidScat has a slightly narrower antenna than QuikSCAT and SeaWinds to account for its lower orbit. The primary differences between the RapidScat data set and data sets from previous pencil-beam scatterometers are due to the nature of RapidScat's orbit. Unlike previous scatterometers, which flew in sun-synchronous orbits where  $\sigma^0$  observations at a given location were collected at exactly two different ltods, the RapidScat orbit is not in a sun-synchronous orbit, which means that the ltod for measurements changes slowly with each orbit through an entire 24 ltod cycle with a periodicity of about two months. While a limitation for some studies, the ltod variation also permits the detailed study of the variation in  $\sigma^0$  with ltod for the first time. We note that the ISS exhibits a much greater variation in attitude than previous scatterometer platforms. As the ISS attitude varies from what RapidScat was designed for, the performance of the fixed-mounted RapidScat instrument is adversely affected. This also results in variations in measurement incidence angle as a function of RapidScat azimuth angle. We note that RapidScat has exhibited very stable and consistent operation, even though its design was optimized for a higher orbit.

In this paper, the standard time-ordered  $\sigma^0$  data product (L1B) is used from each sensor. Only data flagged as usable are used. For RapidScat where the data set is ongoing, the analysis is performed using data from revolutions 161 (October 4, 2014) to 3933 (June 3, 2015) using the "nrt-delayed" data set. The data used are limited to revolutions classified by JPL as "good."

Where appropriate, for each sensor, the data are divided into four separate "flavors" depending on the beam polarization (vertically VV or horizontally HH polarized) and whether the

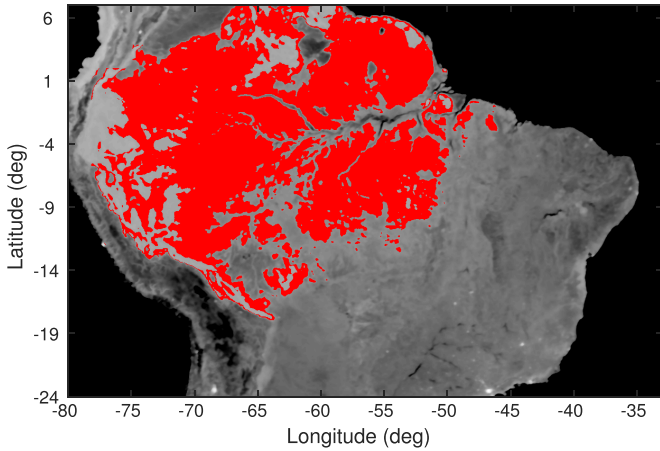


Fig. 1. Spatial mask defining the Amazon rainforest target (red) overlaying a high-resolution QuikSCAT VV polarization  $\sigma^0$  image. Within the mask, the mean for each pixel is within  $\pm 0.5$  dB of the spatial mean.

measurement is acquired during an ascending or descending orbital pass. This is because each beam may have its own bias and the  $\sigma^0$  response for a target varies with the polarization of the beam. Ascending and descending passes take measurements at different ltoads, which may have different  $\sigma^0$  responses due to the diurnal variation of the targets.

### III. EXTENDED AREA TARGETS

The calibration target regions are defined by spatial masks [6]. Only measurements that fall completely in the mask are used. We define two target regions. The Amazon rainforest is used as the primary calibration target, with the Congo rainforest used to confirm the results. In mask creation, the competing demands of homogeneity and size must be balanced. We follow the procedure in [6] and [8] by selecting a region that has a  $\pm 0.5$ -dB range around a nominal  $\sigma^0$ . High-resolution SIR [18] images from the entire QuikSCAT mission are averaged together to generate a single average  $\sigma^0$  image for each of the four flavors of QuikSCAT data. An iterative process is used to find the largest mask for each average  $\sigma^0$  image. Each point that falls within all four intermediate masks is then included in the final mask shown in Fig. 1.

Although selected for their homogeneity, the Amazon and Congo rainforests exhibit small  $\sigma^0$  dependencies on factors such as azimuth angle, incidence angle, time of year, and ltoad. The backscatter response of a distributed target such as the Amazon is too complex to accurately calculate analytically. Therefore, as described hereinafter, empirical models for  $\sigma^0$  dependencies are derived from scatterometer measurements from the various sensor data sets.

#### A. Azimuth Response

Previous studies such as [5], [6], and [9] have shown that the Amazon rainforest is essentially azimuthally isotropic. This can be confirmed for the Amazon and Congo masks by using the ten-year QuikSCAT data set (not shown). It is found that the azimuth dependence is small (less than 0.1 dB in magnitude).

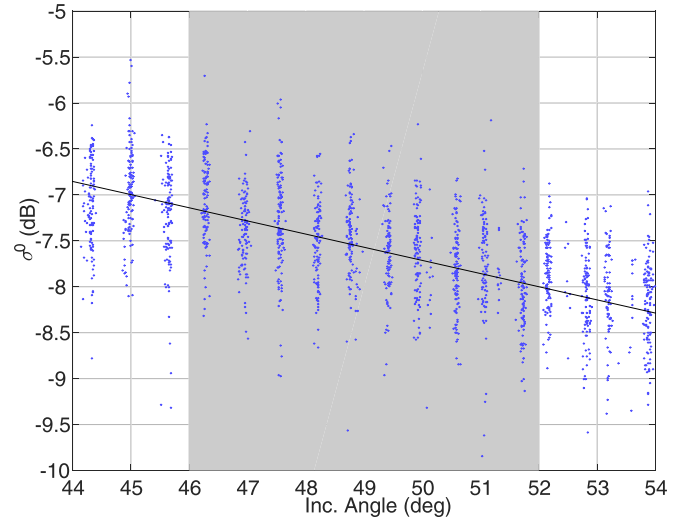


Fig. 2. Scatterplot of incidence angle versus  $\sigma^0$  measured over the Amazon by NSCAT. Horizontally polarized measurements from ascending passes during the NSCAT mission are shown. The shaded area indicates incidence angles of interest for RapidScat calibration (HH-pol). The linear least squares error line for over 600 000 measurements from the shaded area is shown. For plotting clarity, measurements are downsampled for scatterplot.

Most of the sensors sample azimuth angles uniformly for even small sets of data. As a result, any residual azimuth biases tend to average out. Thus, for most comparisons in this paper, azimuth angle dependence due to sampling is neglected.

#### B. Incidence Response

The  $\sigma^0$  response of a distributed natural target generally varies with incidence angle [19]. This must be accounted for when comparing sensors with distinct incidence angles. To do this, we determine the mean incidence angle dependence over our target masks using data from NSCAT and RapidScat.

NSCAT measures  $\sigma^0$  over a wide range of incidence angles for each pulse. A scatterplot of  $\sigma^0$  versus incidence angle over the Amazon mask for NSCAT measurements within the incidence angle range of  $40^\circ$ – $50^\circ$  is shown in Fig. 2. The response of  $\sigma^0$  to incidence is generally nonlinear but can be approximated as linear in decibels over the incidence angle range of interest for RapidScat calibration. This linear relationship is estimated by least squares fitting a line to the data in the incidence range of interest. This is repeated separately for different seasonal windows and polarizations. We found that the slope of the line does not vary significantly with season. We thus average the incidence angle dependence over the NSCAT mission life. The measured dependence is shown in Table II. We note that the NSCAT mission did not cover a full annual cycle; however, given the small variation in the slope observed over the remainder of the year, we do not expect a significant change for the missing months. Given the small incidence angle range for a given beam ( $< 5^\circ$ ), small errors in the estimated slope have only a minimal ( $< 0.1$  dB) impact on the incidence angle correction and thus are neglected. We note that we compared NSCAT-estimated and RapidScat-estimated slopes and found them similar.

TABLE II  
INCIDENCE ANGLE DEPENDENCE (DECIBEL/DEGREE) AS MEASURED BY NSCAT AND RAPIDSCAT. "AVE" DENOTES DAILY AVERAGE, WHILE "ASC" DENOTES ASCENDING ORBIT PASSES AND "DESC" DENOTES DESCENDING ORBIT PASSES

Sensor	Region	HH polarization			VV polarization		
		Ave	Asc	Desc	Ave	Asc	Desc
NSCAT	Amazon	-0.128	-0.135	-0.121	-0.148	-0.143	-0.152
	Congo	-0.232	-0.120	-0.112	-0.137	-0.131	-0.143
RapidScat	Amazon	-0.106			-0.119		
	Congo	-0.101			-0.095		

RapidScat has some ability to measure incidence dependence versus  $\theta_{\text{td}}$  for a narrow range of incidence angles; however, we find no significant dependence on  $\theta_{\text{td}}$ . A mission estimate of incidence dependence is calculated by first estimating incidence dependence for each revolution. These estimates are then averaged using the product of the number of points and the range of incidence covered as a weighting factor. The mission average incidence dependence is included in Table II.

These measured incidence dependencies can be used to normalize measurements taken at various incidence angles to a single nominal incidence angle according to

$$\sigma_{\text{nom}}^0 = \sigma_{\text{meas}}^0 - m(\theta_{\text{meas}} - \theta_{\text{nom}}) \tag{1}$$

where  $\sigma_{\text{meas}}^0$  is the  $\sigma^0$  measurement at incidence angle  $\theta_{\text{meas}}$  and  $\sigma_{\text{nom}}^0$  is the corresponding  $\sigma^0$  at the nominal incidence angle ( $\theta_{\text{nom}}$ ). The term  $m$  is one of the empirical linear corrective terms recorded in Table II. This term varies with the sensor as well as beam due to differences in target incidence dependence for different polarizations as well as sensor-specific incidence-dependent biases.

C. Seasonal Response

QuikSCAT can be used to estimate average seasonal variations in the targets at two discrete  $\theta_{\text{td}}$ s (6 A.M. and 6 P.M.) over its mission life. To estimate the seasonal variation, the data are divided into ten-day bins. For each year of data, the yearly average is subtracted to compute the deviation from the yearly average. These deviations are then averaged across the ten years of QuikSCAT’s mission to yield the mean deviation from the yearly average. Results are averaged over all incidence and azimuth angles. Note that the incidence angle variation of QuikSCAT measurements is very small ( $< 1^\circ$ ). The results are shown in Fig. 3. It is noted that seasonal variations differ between the descending and ascending passes that occur at different  $\theta_{\text{td}}$ s, which suggests that seasonal and diurnal variations are linked. We further note that the seasonal variations are limited to about  $\pm 0.1$  dB and can be compensated for to better than this.

D. Diurnal Response

Due to its orbit, RapidScat is uniquely suited for measuring the diurnal variation of the targets. RapidScat observes the Amazon and Congo rainforest  $\sigma^0$  at a particular  $\theta_{\text{td}}$  on a monthly cycle, as shown for the Amazon in Fig. 4. Averaging

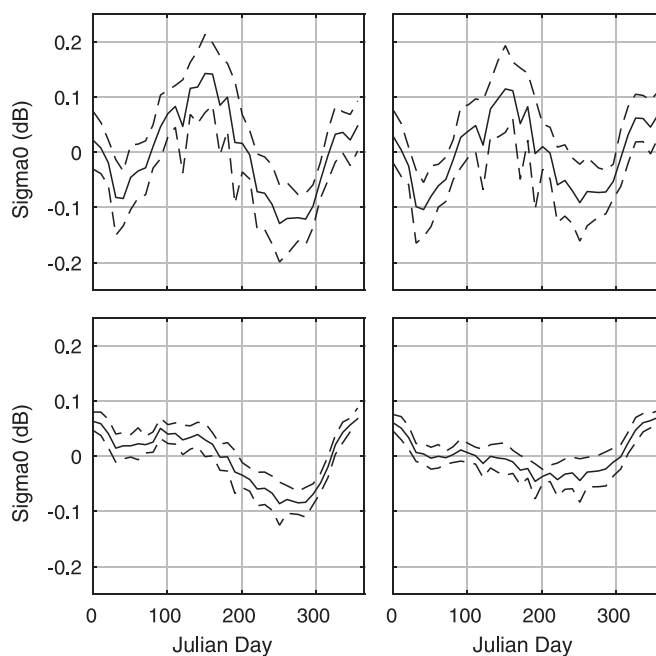


Fig. 3. (Solid lines) Mean deviation from the yearly average for ten-day bins for the Amazon as measured by QuikSCAT. The standard deviation of the averages for each year is indicated with dotted lines. Separate plots are provided for each measurement “flavor.” (ul) Ascending (morning 6 A.M.) pass, HH polarization. (ur) Ascending (morning 6 A.M.) pass, VV polarization. (ll) Descending pass (evening 6 P.M.), HH polarization. (lr) Descending (evening 6 P.M.) pass, VV polarization. While there is a seasonal cycle with an amplitude of  $\sim 0.1$  dB, the interannual variation is less than  $\pm 0.1$  dB, which suggests that the Amazon region is remarkably stable from year to year when averaged over the mask region.

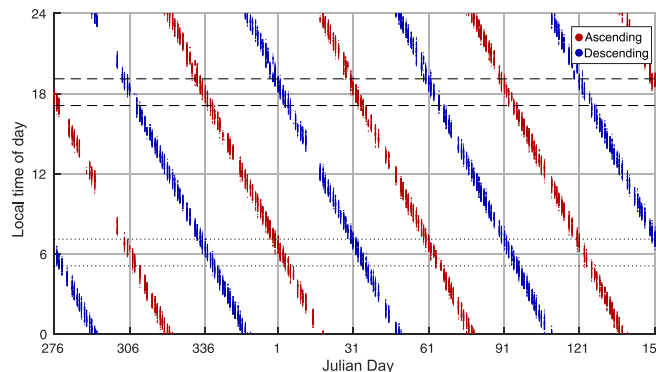


Fig. 4. Scatterplot of  $\theta_{\text{td}}$  of RapidScat measurements over the Amazon mask from August 2014 to May 2015. The slope of the pattern is approximately 24 h per 60 days. For comparison with the sun-synchronous QuikSCAT, the dotted lines show the span of the local time of the ascending orbit passes, while the dashed lines show the span of the descending orbit passes.

these monthly samples for each  $\theta_{\text{td}}$  yields the graphs seen in Fig. 5. There is a clear peak in average  $\sigma^0$  near sunrise. This can be attributed to dew accumulation on the leaves of the canopy [5], [10]. Taking the standard deviation of the monthly samples provides a rough estimate for the magnitude of the seasonal variation at that  $\theta_{\text{td}}$ . The standard deviation is shown with the dotted lines in Fig. 5. It can be seen that, at least for the Amazon, the deviation is greatest around 6 A.M. where the seasonal variation measured by QuikSCAT is greater. This suggests that some of the seasonal variation in QuikSCAT  $\sigma^0$  at this time may be due to aliased diurnal cycling and variability.

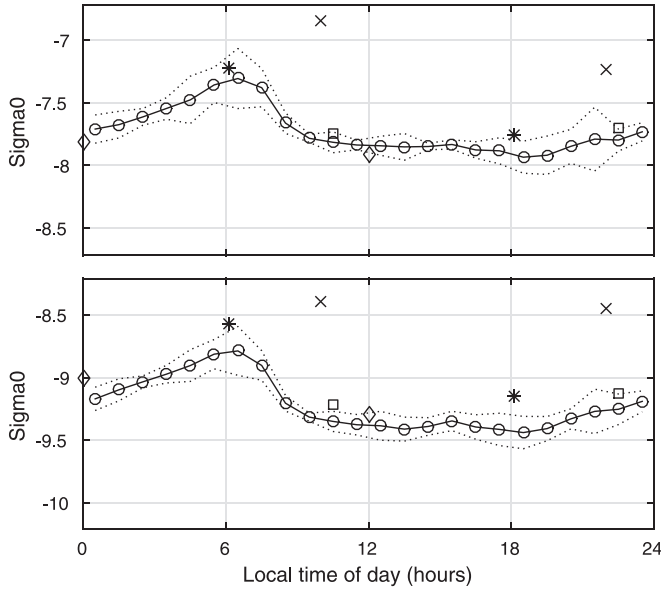


Fig. 5. Mean diurnal  $\sigma^0$  response of the Amazon as measured by RapidScat ( $\circ$  connected by the solid line). (Top panel) HH polarization. (Bottom panel) VV polarization. Dotted lines indicate the standard deviation of the averages of each monthly sample of the diurnal signal. Mission averages are also shown for NSCAT ( $\times$ ), QuikSCAT ( $*$ ), SeaWinds ( $\square$ ), and OSCAT ( $\diamond$ ). All measurements have been normalized to QuikSCAT incidence angles. The NSCAT value is computed by using only  $\sigma^0$  values within  $2.5^\circ$  of the nominal QuikSCAT incidence angle. The other sensor values have been adjusted to the QuikSCAT incidence using the NSCAT-derived incidence angle correction factor. The diurnal cycle is several tenths of a decibel and peaks at roughly 6 A.M. local time. Note that most of the differences between the sensor mean  $\sigma^0$  values can be explained by the diurnal cycle and a mean calibration offset.

This is the first time the full diurnal  $\sigma^0$  cycle of the Amazon or the Congo has been measured with a single sensor at wind scatterometer incidence angles. Fig. 5 shows the averages for QuikSCAT ascending and descending passes. The *difference* between the averages is well predicted by the diurnal signal measured by RapidScat. The SeaWinds and OSCAT averages also correspond well to the diurnal signal. The same can be said for the OSCAT averages, although there is a larger variation for OSCAT vertically polarized ascending passes at midnight.

#### IV. RESULTS

As noted, the responses of the calibration targets exhibit dependencies on azimuth angle, incidence angle, season, and local time. We consider a number of strategies to account for dependencies.

One strategy is to limit the data used for comparison. For example, QuikSCAT only measures  $\sigma^0$  at two distinct ltods, while RapidScat  $\sigma^0$  measurements span all ltods. To compare the two sensors, RapidScat measurements with ltod near the QuikSCAT ltod are used. This approach does not use all of the data and so has fewer points to average, but it does effectively eliminate the dependence.

Another strategy is to average out the dependence. This is suitable for a dependence such as the azimuth angle. Azimuth angles are sampled relatively uniformly with respect to all the other dependencies. As a result, even small sample sets contain

TABLE III  
DIFFERENCE BETWEEN RAPIDSCAT AVERAGE  $\sigma^0$  FOR 6 A.M. (MORNING) AND 6 P.M. (EVENING) AND QUIKSCAT MEAN ASCENDING AND DESCENDING  $\sigma^0$  USING A VARIETY OF METHODS. SEE TEXT FOR DESCRIPTION OF METHODS. THE NEGATIVE VALUES SUGGEST THAT RAPIDSCAT IS BIASED LOW RELATIVE TO QUIKSCAT

Method	Region	6 a.m.		6 p.m.	
		HH	VV	HH	VV
1	Amazon	-0.12	-0.23	-0.17	-0.29
	Congo	-0.07	-0.21	-0.10	-0.25
2	Amazon	-0.08	-0.22	-0.14	-0.29
	Congo	-0.03	-0.20	-0.08	-0.26
3	Amazon	-0.08	-0.23	-0.14	-0.29
	Congo	-0.03	-0.22	-0.08	-0.26
4	Amazon	-0.13	-0.27	-0.19	-0.33
	Congo	-0.17	-0.30	-0.15	-0.29

a full range of azimuth angles. Since the azimuth dependence is also very small, any residual imbalances in the sampling do not create significant biases.

The third strategy is to apply corrective factors to adjust both data sets to a nominal value. This is often the last choice, but it is necessary when the previous strategies are not feasible. This is the method used for incidence angle dependence: A nominal incidence angle is chosen, and all measurements are normalized to that value. This incidence angle correction works well because there is a good understanding of the incidence angle dependence in the range of incidence angles of interest (from NSCAT and RapidScat) and because the incidence angle dependence does not change significantly with other variables.

These strategies are applied to various sets of data to arrive at the results in this section.

##### A. Mean Bias Estimates

QuikSCAT is the standard scatterometer to which other Ku-band scatterometers are compared. We use four different methods to estimate the biases between QuikSCAT and RapidScat.

The first method produces a single RapidScat average  $\sigma^0$  corresponding to the mission average for each flavor of QuikSCAT  $\sigma^0$ . Incidence angle is corrected using the correction factors from Table II according to (1). RapidScat measurements are limited to within 1 h of the corresponding QuikSCAT local times as shown in Fig. 4. Azimuth variations are averaged out. QuikSCAT is limited to ten complete years of data, resulting in an annual average  $\sigma^0$ . Since the RapidScat data set does not cover a full year, we apply seasonal corrections based on QuikSCAT measurements (see Fig. 3). The estimated annual average  $\sigma^0$  are then compared. This comparison is shown in Table III as method 1.

The second method is very similar to the first, except that the QuikSCAT data used are limited to the times of year covered by RapidScat. This way, both data sets cover the same seasons, and any seasonal dependence can be averaged out instead of applying a seasonal correction to RapidScat. The resulting bias estimates can be seen in Table III as method 2.

In the third method, instead of averaging over the full mask, we account for spatial variability by splitting the masked data

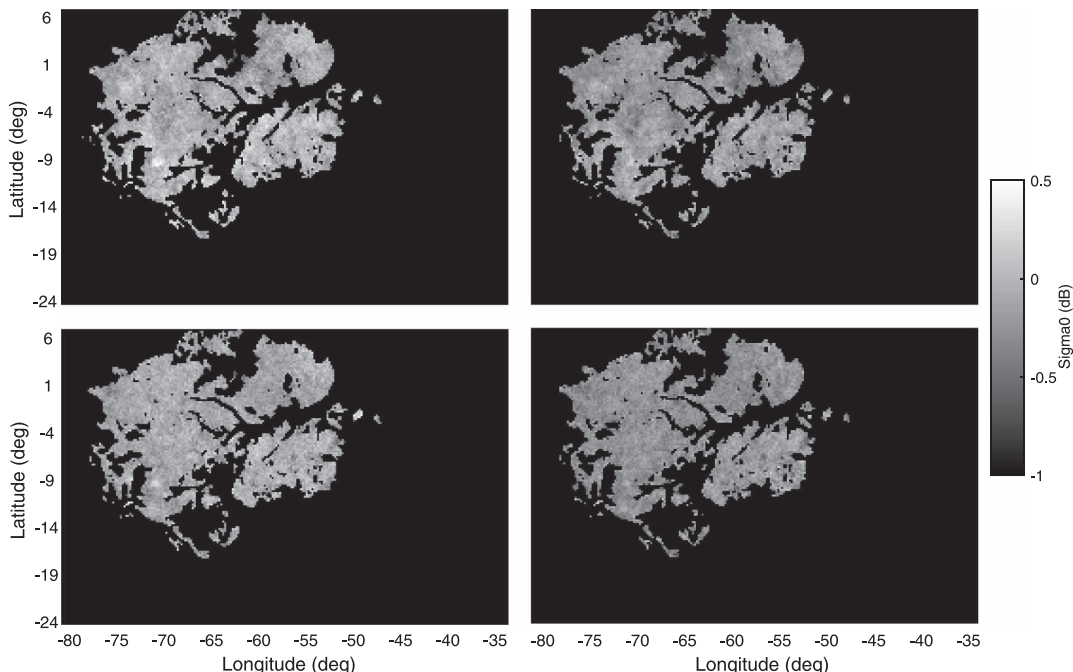


Fig. 6. Images of the differences (in decibels) of the QuikSCAT average  $\sigma^0$  in 2008 and RapidScat mission average  $\sigma^0$  within the Amazon mask. RapidScat is normalized to the nominal QuikSCAT incidence angle before comparison using RapidScat-observed incidence angle dependence. (ul) Morning (6 A.M.) pass, HH polarization. (ur) Morning (6 A.M.) pass, VV polarization. (ll) Evening (6 P.M.) pass, HH polarization. (lr) Evening (6 P.M.) pass, VV polarization. Note that the differences are essentially spatially constant over the mask region for each case.

into  $0.2^\circ$  by  $0.2^\circ$  latitude–longitude zones (subregions) and then comparing. This produces a different estimate of the bias for each spatial zone within the mask. A benefit of this spatial comparison is the identification of regions that experience significant change in average  $\sigma^0$  between the QuikSCAT and RapidScat missions due to factors such as deforestation. In Fig. 6, no significant regional differences are seen. This suggests that, between 2008 and 2015, no regions in the mask experienced enough change to noticeably decrease the backscatter response [15]. Histograms of the differences are shown in Fig. 7. Averaging the bias estimates for every year of QuikSCAT data yields the overall bias estimates shown in Table III as method 3.

The fourth method is to split the RapidScat data by day of year (season) and then compare those averages with QuikSCAT averages taken from the same day of year. RapidScat only measures the target at QuikSCAT ltod approximately once per month if both ascending and descending passes are used as seen in Fig. 4. This is due to the two-month cycle in RapidScat ltod of measurements. The dotted lines in Fig. 4 indicate the range of RapidScat ltoDs that are used for comparison with QuikSCAT. Each monthly group of measurements is taken at a distinct range of day of year, averaged, and compared with the QuikSCAT average for the same day range. The results are shown in Fig. 8 and provide a separate estimate of bias between QuikSCAT and RapidScat for every month during the RapidScat mission life. These can be used to estimate potential instrumental drift in RapidScat. Some of the variability may be due to geophysical differences such as rain. There are no clear trends in the bias or any distinct outliers suggesting that RapidScat is stable. There does, however, seem to be a pattern

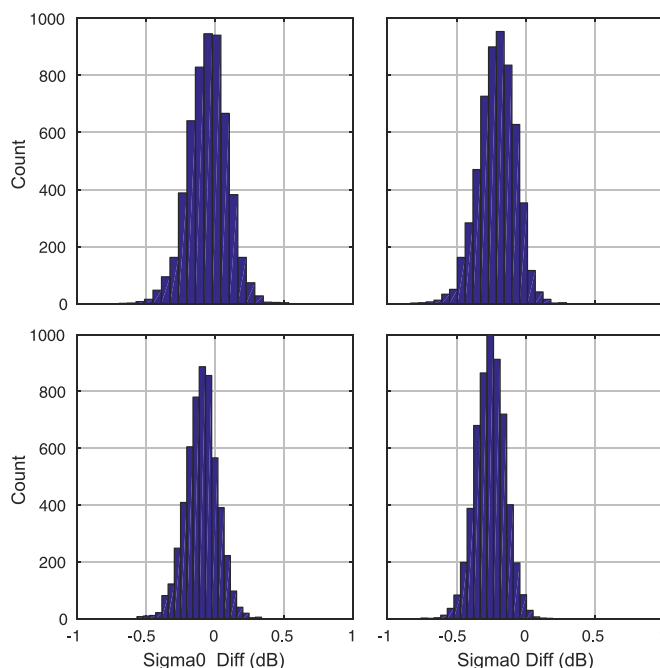


Fig. 7. Histograms of the differences (in decibels) between the QuikSCAT average  $\sigma^0$  in 2008 and RapidScat mission average  $\sigma^0$  within the Amazon mask shown in Fig. 6. (ul) Morning (6 A.M.) pass, HH polarization. (ur) Morning (6 A.M.) pass, VV polarization. (ll) Evening (6 P.M.) pass, HH polarization. (lr) Evening (6 P.M.) pass, VV polarization.

of alternating bias estimates. There is no definite explanation for such behavior, and we are uncertain of its cause. By averaging the bias estimates, we obtain a single mean bias offset for each mask and flavor, shown in Table III as method 4.

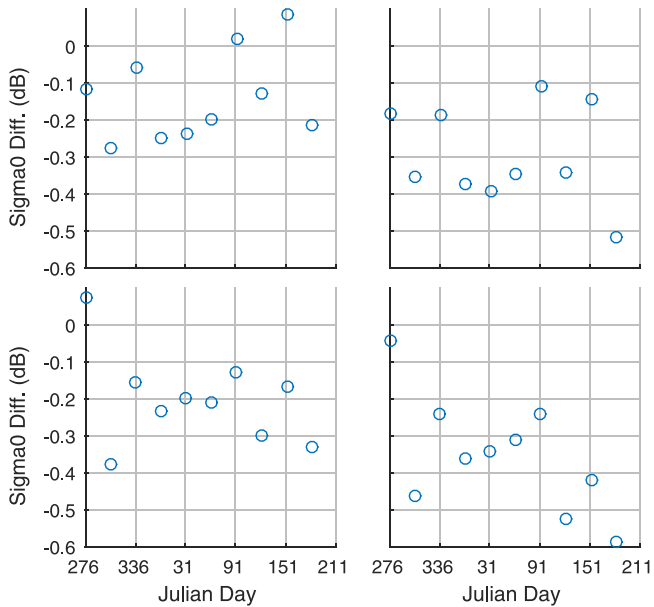


Fig. 8. Differences between RapidScat mean  $\sigma^0$  for different times of year and the QuikSCAT average for the same time of year (season) over the Amazon. RapidScat is normalized to the nominal QuikSCAT incidence angle before comparison using RapidScat-observed incidence angle dependence. Separate plots are provided for each measurement “flavor.” (ul) Morning (6 A.M.) pass, HH polarization. (ur) Morning (6 A.M.) pass, VV polarization. (ll) Evening (6 P.M.) pass, HH polarization. (lr) Evening (6 P.M.) pass, VV polarization.

The results of the four different methods to estimate the biases between QuikSCAT and RapidScat are shown in Table III. While each apply the same strategy for azimuth, diurnal, and incidence dependencies, they have varied strategies with regard to seasonal and spatial dependencies. All the estimates suggest that RapidScat is biased low compared to QuikSCAT. All of the methods also agree that the bias is smaller for the horizontally polarized beam (0–0.2 dB) than it is for the vertically polarized beam (0.2–0.3 dB).

### B. Yearly Averages

When comparing QuikSCAT and RapidScat, there is the possibility that the scattering characteristics of the targets may have changed in the time between the two missions. Although no regions stand out in Fig. 6, there is the possibility of larger scale vegetation or climate changes that affect the whole region. In order to address this and also to compare  $\sigma^0$  from different Ku-band scatterometers, we examine the year-to-year behavior of the calibration targets as measured by NSCAT, QuikSCAT, QuikSCAT PWM, OSCAT, SeaWinds, and RapidScat.

The readings from each sensor are normalized to correspond to QuikSCAT yearly average  $\sigma^0$  for comparison. RapidScat measurements used are limited to QuikSCAT ltod. Measurements from other sensors have a ltod correction applied using the diurnal cycle measured by RapidScat (see Fig. 5). Measurements from all sensors are normalized to the QuikSCAT incidence angle. An azimuth correction is also applied to QuikSCAT PWM data. Seasonal corrections are applied to RapidScat and QuikSCAT PWM according to the results in Fig. 3. The resulting multiannual comparison is shown in Fig. 9.

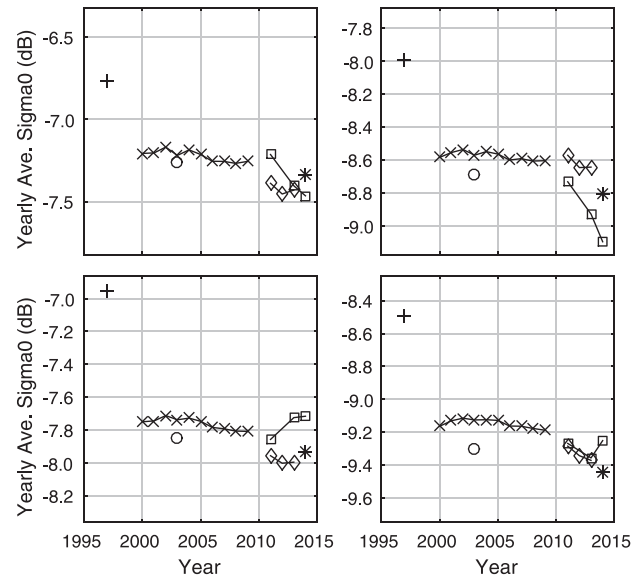


Fig. 9. Yearly average  $\sigma^0$  for QuikSCAT ( $\times$ ), QuikSCAT PWM data ( $\square$ ), RapidScat ( $*$ ), SeaWinds ( $\circ$ ), OSCAT ( $\diamond$ ), and NSCAT ( $+$ ) over the Amazon. Separate plots are provided for each measurement “flavor.” (ul) Ascending pass, HH polarization. (ur) Ascending pass, VV polarization. (ll) Descending pass, HH polarization. (lr) Descending pass, VV polarization. Note that different sensors have different local times of day for each pass. An LTOD correction based on RapidScat has been applied to OSCAT, SeaWinds, and NSCAT to QuikSCAT times. The RapidScat value is shown for QuikSCAT times. The nearly flat QuikSCAT curve reveals how stable the Amazon is over time. The vertical offset of the different sensors reflects their relative calibration bias and their differences in ltod. Some of the differences could be due to imperfections in the ltod correction.

In Fig. 9, several things are notable. The first is that the backscatter response as measured by QuikSCAT is remarkably stable with a year-to-year variation of no more than 0.1 dB. Also, the SeaWinds, OSCAT, and RapidScat measurements are all within 0.3 dB of the QuikSCAT averages, suggesting a relatively accurate cross-calibration despite the difference in ltod of the original measurements. At the same time, the biases are large enough that it is unlikely that they are attributable solely to yearly variation in the target. The QuikSCAT PWM has some inconsistent behavior, probably attributable to the limited amount of incidence angles available and the limitations of corrections that were applied. NSCAT  $\sigma^0$  appears to be biased high compared to other sensors. This may, in part, be due to the difference in frequency between NSCAT and the other sensors (see Table I).

### C. Slice Balancing

As with QuikSCAT [4], an estimated azimuth-dependent bias correction is applied to the RapidScat data by JPL. Unfortunately, the RapidScat correction is not as effective as the QuikSCAT correction. This appears to be due in large measure to variations in the pitch of the ISS. After accounting for incidence angle, each slice should have the same average  $\sigma^0$  as the egg measurements, and azimuth variation should be less than 0.1 dB. After careful examination of the slice measurements, we find that the applied slice balancing is most effective when the ISS pitch is close to that for which the slice balance was

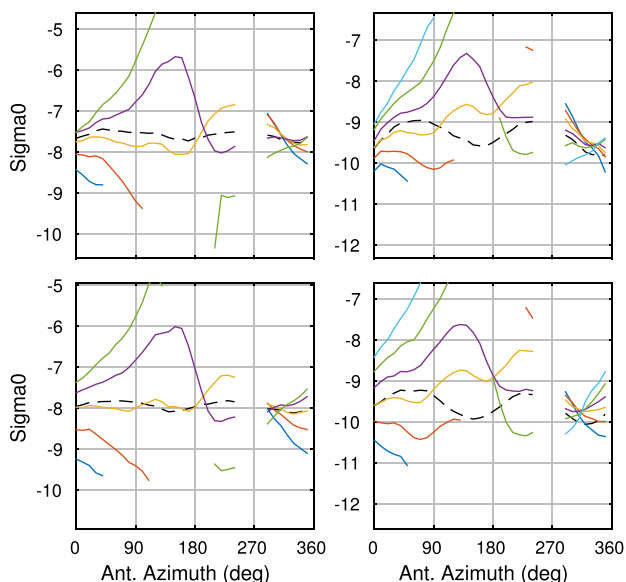


Fig. 10. Average  $\sigma^0$  over the Amazon for the six inner slices and the egg measurement (dashed line) for days 169–185, 2015. Note the gap in data near  $270^\circ$  azimuth due to ISS geometry. Gaps are also present for individual slices when the slices fall out of the range gate. Slice balancing has been applied to the data, but the mean pitch of  $2.74^\circ$  is far from that for which the slice balancing is based. The  $\sigma^0$  shown has been normalized to QuikSCAT incidence angles. Separate plots are provided for each measurement “flavor.” (ul) Ascending pass, HH polarization. (ur) Ascending pass, VV polarization. (ll) Descending pass, HH polarization. (lr) Descending pass, VV polarization. The wide fluctuation of the slice values from the egg value suggests that the slice balancing is ineffective when the attitude is far from that for which the slice balancing is designed.

designed. However, when the ISS pitch is several degrees off from what the slice balance is set for, the balancing does not perform well. The azimuth response for each slice at such a time is shown in Fig. 10. Here, we see large azimuth biases on the order of several decibels for the slice measurements, and we conclude that the slices are not well balanced for large ISS pitch variations.

Another problematic symptom of the high pitch is egg azimuth dependence, as illustrated in Fig. 10. Azimuth dependence for egg measurements is not present when the ISS pitch is close to nominal. However, for large pitch angles, it becomes significant. In Fig. 10, there are two minima visible in the azimuth response. There is a coupling between azimuth angle and incidence angle due to the pitch of the ISS, and these minima correspond to azimuth angles that have either higher or lower incidence angles. The lower apparent  $\sigma^0$  at these extreme incidence angles can possibly be attributed to changes in the slant range to target and resultant range-gate clipping within the RapidScat system. (Recall that the SeaWinds design was originally optimized for higher altitude operation and can produce range-gate clipping when operated at the ISS altitude.) Range-gate clipping is the loss of signal power when a portion of the signal does not fall within the receive window. If range-gate clipping is not properly accounted for during  $\sigma^0$  retrieval, the measured  $\sigma^0$  will be biased. This behavior should be considered when using RapidScat data taken during extreme ISS pitch regimes as it may result in biases in the estimated wind over the ocean.

## V. CONCLUSION

Data from multiple Ku-band scatterometers are used to characterize the azimuth, incidence, seasonal, and diurnal dependencies present in two natural land targets: the Amazon and Congo rainforests. These dependencies are then used to compare  $\sigma^0$  readings between different scatterometers, particularly RapidScat and QuikSCAT.

The azimuth dependence of the targets is measured using QuikSCAT and is found to be less than  $\pm 0.1$  dB. Incidence dependence is measured using RapidScat and NSCAT data. The estimates agree reasonably well. Differences between the RapidScat and NSCAT measurements can be attributed to differences in  $\sigma^0$  retrieval and azimuth balancing between the two systems. The seasonal dependence of the rainforests is measured over multiple years using QuikSCAT and is estimated to be less than  $\pm 0.25$  dB. By accounting for the average seasonal variation as well as *ltod*, the residual interannual variation may be reduced to less than  $\pm 0.1$  dB, which suggests that these targets are suitable for use in the calibration of sensors using data from disjoint years and are superior to ice regions also used for scatterometer calibration [20].

RapidScat enables the measurement of the diurnal dependence over the Amazon and Congo rainforests. The significant diurnal signal is found to be almost  $\pm 0.5$  dB in magnitude. The measured diurnal cycle explains the differences seen in the mean  $\sigma^0$  between QuikSCAT’s and other sensors’ ascending and descending passes. It also enables better comparison between sensors that collected measurements at different *ltods*.

The observed dependencies are used to create empirical models for  $\sigma^0$  response of the calibration targets. The empirical models are used to validate the RapidScat data record. Slice balancing is evaluated by applying an incidence angle correction and examining the azimuth response of each slice. We find that the effectiveness of the slice balancing depends strongly on the pitch of the ISS. The long-term stability of RapidScat is evaluated by applying a diurnal, seasonal, and incidence angle correction to RapidScat data and then comparing RapidScat data from different times during its mission to corresponding QuikSCAT data. There is limited change in the mean  $\sigma^0$  over the RapidScat mission life using this method, confirming that RapidScat is stable relative to QuikSCAT.

The empirical models are also used to account for differences in characteristics between sensors, allowing the estimation of relative instrumental biases. Yearly average  $\sigma^0$  values are found for NSCAT, QuikSCAT, QuikSCAT PWM, SeaWinds, OSCAT, and RapidScat after compensating for differences in incidence angle, azimuth angle, *ltod*, and time of year. Different methods are explored for estimating mean biases between RapidScat and QuikSCAT. RapidScat is estimated to be biased slightly low compared to QuikSCAT. The magnitude of the bias varies with the estimation method and ranges from 0.02–0.19 dB for H-pol and 0.20–0.33 dB for V-pol.

## REFERENCES

- [1] F. Naderi, M. Freilich, and D. Long, “Spaceborne radar measurement of wind velocity over the ocean—An overview of the NSCAT scatterometer system,” *Proc. IEEE*, vol. 79, no. 6, pp. 850–866, Jun. 1991.
- [2] M. H. Freilich, D. G. Long, and M. W. Spencer, “SeaWinds: A scanning scatterometer for ADEOS-II-science overview,” in *Proc. IEEE IGARSS*

- Surface Atmos. Remote Sens., Technol., Data Anal. Interpretation*, 1994, vol. 2, pp. 960–963.
- [3] J. E. Graf, W. Tsi, and L. Jones, “Overview of QuikSCAT mission—a quick deployment of a high resolution, wide swath scanning scatterometer for ocean wind measurement,” in *Proc. IEEE Southeastcon*, 1998, pp. 314–317.
- [4] J. N. Huddleston, W. Tsai, M. W. Spencer, B. W. Stiles, and R. S. Dunbar, “SeaWinds on QuikSCAT: Postlaunch calibration and validation,” in *Proc. IEEE IGARSS*, 2000, vol. 3, pp. 1024–1026.
- [5] I. Birrer, E. Bracalente, G. Dome, J. Sweet, and G. Berthold, “ $\sigma^0$  signature of the Amazon rain forest obtained from the Seasat scatterometer,” *IEEE Trans. Geosci. Remote Sens.*, vol. GE-20, no. 1, pp. 11–17, Jan. 1982.
- [6] D. G. Long and G. B. Skouson, “Calibration of spaceborne scatterometers using tropical rain forests,” *IEEE Trans. Geosci. Remote Sens.*, vol. 34, no. 2, pp. 413–424, Mar. 1996.
- [7] W. Tsai *et al.*, “Postlaunch sensor verification and calibration of the NASA scatterometer,” *IEEE Trans. Geosci. Remote Sens.*, vol. 37, no. 3, pp. 1517–1542, May 1999.
- [8] J. Zec, D. G. Long, and W. L. Jones, “NSCAT normalized radar backscattering coefficient biases using homogenous land targets,” *J. Geophys. Res., Oceans*, vol. 104, no. C5, pp. 11 557–11 568, May 1999.
- [9] J. Zec, W. L. Jones, and D. G. Long, “SeaWinds beam and slice balance using data over Amazonian rainforest,” in *Proc. IEEE IGARSS*, 2000, vol. 5, pp. 2215–2217.
- [10] L. B. Kunz and D. G. Long, “Calibrating SeaWinds and QuikSCAT scatterometers using natural land targets,” *IEEE Geosci. Remote Sens. Lett.*, vol. 2, no. 2, pp. 182–186, Apr. 2005.
- [11] J. C. Barrus, “Intercalibration of QuikSCAT and OSCAT land backscatter,” M.S. thesis, Ira A. Fulton College Eng. Technol.; Elect. Comput. Eng., Brigham Young Univ., Provo, UT, USA, 2013.
- [12] S. A. Bhowmick, R. Kumar, and A. K. Kumar, “Cross calibration of the OceanSAT-2 scatterometer with QuikSCAT scatterometer using natural terrestrial targets,” *IEEE Trans. Geosci. Remote Sens.*, vol. 52, no. 6, pp. 3393–3398, Jun. 2014.
- [13] R. Kumar, S. A. Bhowmick, K. Babu, R. Nigam, and A. Sarkar, “Relative calibration using natural terrestrial targets: A preparation toward Oceansat-2 scatterometer,” *IEEE Trans. Geosci. Remote Sens.*, vol. 49, no. 6, pp. 2268–2273, Jun. 2011.
- [14] R. G. Kennett and F. K. Li, “Seasat over-land scatterometer data. II. Selection of extended area and land-target sites for the calibration of spaceborne scatterometers,” *IEEE Trans. Geosci. Remote Sens.*, vol. 27, no. 6, pp. 779–788, Nov. 1989.
- [15] S. Jaruwatanadilok and B. W. Stiles, “Trends and variation in Ku-band backscatter of natural targets on land observed in QuikSCAT data,” *IEEE Trans. Geosci. Remote Sens.*, vol. 52, no. 7, pp. 4383–4390, Jul. 2014.
- [16] M. W. Spencer, C. Wu, and D. G. Long, “Improved resolution backscatter measurements with the SeaWinds pencil-beam scatterometer,” *IEEE Trans. Geosci. Remote Sens.*, vol. 38, no. 1, pp. 89–104, Jan. 2000.
- [17] M. A. Bourassa, E. Rodriguez, and R. Gaston, “NASA’s ocean vector winds science team workshops,” *Bull. Amer. Meteorol. Soc.*, vol. 91, no. 7, pp. 925–928, Jul. 2010.
- [18] D. S. Early and D. G. Long, “Image reconstruction and enhanced resolution imaging from irregular samples,” *IEEE Trans. Geosci. Remote Sens.*, vol. 39, no. 2, pp. 291–302, Feb. 2001.
- [19] F. T. Ulaby and D. G. Long, *Microwave Radar and Radiometric Remote Sensing*. Ann Arbor, MI, USA: Univ. Michigan Press, 2014.
- [20] K. Moon and D. G. Long, “Considerations for Ku-band scatterometer calibration using the dry snow zone of the Greenland ice sheet,” *IEEE Geosci. Remote Sens. Lett.*, vol. 10, no. 6, pp. 1344–1349, Nov. 2013.



**Nathan M. Madsen** (M’15) received the M.S. degree in electrical engineering from Brigham Young University, Provo, UT, USA, in 2015. While there, he performed research with the BYU Microwave Earth Remote Sensing Laboratory.

He recently joined Rincon Research Inc., in Tucson, Arizona.



**David G. Long** (S’80–SM’98–F’08) received the Ph.D. degree in electrical engineering from the University of Southern California, Los Angeles, CA, USA, in 1989.

From 1983 to 1990, he worked for NASA’s Jet Propulsion Laboratory (JPL) where he developed advanced radar remote sensing systems. While at JPL, he was the Project Engineer on the NASA Scatterometer project which flew from 1996 to 1997. He also managed the SCANSAT project, the precursor to SeaWinds which was flown in 1999 on QuikSCAT,

in 2002 on ADEOS-II, and in 2014 on the International Space Station. He is currently a Professor in the Electrical and Computer Engineering Department at Brigham Young University, Provo, UT, USA, where he teaches upper division and graduate courses in communications, microwave remote sensing, radar, and signal processing and is the Director of the BYU Center for Remote Sensing. He is the principal investigator on several NASA-sponsored research projects in remote sensing. He has over 400 publications in various areas, including signal processing, radar scatterometry, and synthetic aperture radar. His research interests include microwave remote sensing, radar theory, space-based sensing, estimation theory, signal processing, and mesoscale atmospheric dynamics.

Dr. Long has received the NASA Certificate of Recognition several times and is an Associate Editor for the IEEE GEOSCIENCE AND REMOTE SENSING LETTERS.